J Solid State Electrochem (2010) 14:197–202
DOI 10.1007/s10008-009-0825-2

ORIGINAL PAPER

Synthesis, electrochemical, and gas sensitivity performance of polyaniline/MoO_3 hybrid materials

Xin Wei · Lifang Jiao · Junli Sun · Sichen Liu · Huatang Yuan

Received: 22 December 2008 / Revised: 27 February 2009 / Accepted: 4 March 2009 / Published online: 29 April 2009

Abstract Hybrid material of polyaniline with molybdenum trioxide (MoO_3) xerogel obtained by ion exchange of $(NH_4)_6Mo_7O_{24}{\cdot}4H_2O$ was synthesized via polymerization of the monomer by ammonium peroxydisulfate/HCl oxidant system. The properties of MoO_3 and hybrid material were investigated through thermogravimetry, X-ray diffraction, scanning electron microscopy, charge–discharge test, cyclic voltammetry, electrochemical impedance spectroscopy, and gas sensing experiments. Results show that hybrid material exhibits higher capacity, more excellent cycling reversibility, and better sensitivity to ethanol gas than MoO_3 xerogel.

Keywords Hybrid · Polyaniline · Molybdenum oxide · Cathode materials · Lithium-ion batteries

Introduction

Organic–inorganic hybrid materials based on conducting polymers and transition metal oxides have attracted great interest during recent years because of their potential for use as active components in electrode material in lithium batteries [1–3]. Furthermore, they possess the advantages of both components and may exhibit advanced properties via the modification of each other [4–7].

Polyaniline (PANI) as the conducting polymer has been widely studied with respect to facile synthesis by chemical and electrochemical process, environmental stability, low cost, high conductivity, solubility, and chemical sensitivity [8]. It has an increasing number of applications in various technologic fields, including electrochromic devices, electrochemical super capacitors, batteries, biosensors, and corrosion inhibitors [9, 10].

It is known that molybdenum trioxide (MoO_3) is a typical host for many monovalent and multivalent cations inserted chemically or electrochemically. The insertion suitability of MoO_3 is due to its layered crystal structure. Edge- and corner-sharing [MoO_6] octahedra build up double layers, and these layer planes characterized by strong covalent bonds are held together by weak van der Waals attraction forces. Objective ions such as Li^+ easily go into interlayers. The layered structure can be kept during the process of intercalation/deintercalation of lithium ion [11]. MoO_3 has been found to be very sensitive to various gases such as NO, NO_2, C_2H_5OH [12], CO, H_2, and NH_3 in temperature range of 300–600 °C [13–15].

Many researchers have synthesized hybrid materials of MoO_3 and PANI. It was reported that polymerization of ANI can be conventionally achieved by using $(NH_4)_2S_2O_8$/HCl as the oxidant system [16]. Ballav et al. recently prepared $(PANI)_xMoO_3$ in the presence of ammonium vanadate/H_2SO_4 oxidant system [17].Toshio Itoh and co-workers accommodated PANI into MoO_3 interlayers by ion-exchange process, using $[Na(H_2O)_2]_xMoO_3$ and aniline monomer as reactant [18]. Xiao-Xia Liu et al. synthesized composite films of PANI and molybdemum oxide by

X. Wei · L. Jiao (✉) · J. Sun · S. Liu · H. Yuan
Institute of New Energy Material Chemistry, Nankai University, Tianjin 300071, People's Republic of China
e-mail: jiaolf@nankai.edu.cn

X. Wei · L. Jiao · J. Sun · S. Liu · H. Yuan
Engineering Research Center of Energy Storage & Conversion (Ministry of Education), Nankai University, Tianjin 300071, People's Republic of China

X. Wei · L. Jiao · J. Sun · S. Liu · H. Yuan
Key Laboratory of Energy-Material Chemistry (Tianjin), Nankai University, Tianjin 300071, People's Republic of China

electrocodeposition in aqueous media, using aniline and $(NH_4)_6Mo_7O_{24}$ as precursors [19]. Junzhong Wang et al. obtained $(PANI)_xMoO_3$ by an ex situ intercalation process [20]. Ballav and Biswas synthesized composite of polyaniline with MoO_3 via polymerization of aniline monomer by ammonium vanadate/H_2SO_4 oxidant system in presence of an aqueous suspension of MoO_3 [17]. Yu and co-workers prepared $(PANI)_xMoO_3$ by direct intercalation of conducting polymer macromolecules [3]. But, modifying MoO_3 xerogel obtained by ion-exchange process with polyaniline intercalated has not been reported.

In this work, we synthesized hybrid material of polyaniline and molybdenum trioxide (MoO_3) xerogel, of which MoO_3 was obtained by ion-exchange process. This hybrid material was prepared via polymerization of the monomer with chemical oxidant method, and it exhibited homogeneous morphology. Electrochemical property and gas sensing property were thoroughly investigated.

Experimental

A clear light-blue MoO_3 sol. (pH=1.0) was prepared by an ion exchange of $(NH_4)_6Mo_7O_{24}\cdot 4H_2O$ (≥99.0%) through a cation exchange resin (from Tianjin NanKai Hecheng S&T). The MoO_3 sol. was dried to a gel under constant heating and stirring to evaporate water, and then, light-blue white MoO_3 xerogel was obtained.

Ammonium peroxydisulfate was dissolved in hydrochloric acid. A quantitative amount of MoO_3 xerogel was added in the solution and sonicated for 30 min, and then, a white colored suspension was formed. A quantitative amount of aniline monomer distilled under reduced pressure and stored in dark prior to use was dissolved in an organic solvent (CCl_4).The two solutions were then carefully transferred to a beaker, with an interface generated between the two layers [17, 21]. The system was stirred with a magnetic stirrer for 24 h at room temperature. The color of the suspension gradually changed from white to light brown and finally to dark brown. The precipitation was filtered and washed with distilled water, ethanol, and acetone. The solid product was vacuum-dried at 50 °C for 2 h.

The hybrid material was analyzed by thermogravimetry (TG) using NETZSCH TG209. The result was obtained in N_2.

The X-ray diffraction (XRD) patterns of MoO_3 and $(PANI)_xMoO_3$ were investigated using a Rigaku D/MAX-2500 powder diffractometer with a graphite monochromatic Cu Kα radiation (λ=0.15406 nm) in the 2 range of 3–80°.

Scanning election microscope (SEM) images of the samples were obtained on the FEG SEM Sirion scanning electron microscope used to observe morphology, size, and distribution.

Electrochemical measurements were carried out with lithium metal as anode electrodes and cathode materials were fabricated by mixing 80% of the active material with 10% carbon black and 10% PTFE. The electrolytes were 1 M $LiPF_6$ dissolved in EC+DMC (1:1 volume ratio) and separator was Celgard 2300 film. The testing cells were assembled in an argon-filled glove box (home-made) in which water and oxygen concentration was kept less than 5 ppm. The discharge–charge tests were run at a current density of 100 mA g^{-1} at the potential range of 1.0–4.2 V. All the tests were performed at room temperature.

Cyclic voltammetry (CV) tests and electrochemical impedance spectroscopy (EIS) experiments were performed on a CHI660B electrochemical workstation. CV was tested at a scan rate of 0.1 mV s^{-1} on the voltage range 1.0–4.2 V (versus $Li|Li^+$). In the EIS experiments, ac perturbation signal was ±5 mV, and the frequency range was from 10 mHz to 105 Hz. The impedance spectrums were analyzed by using Z-View software from Scribner Associates.

Gas sensing tests were carried on WS-30A Winsen gas sensor (from Zhengzhou Winsen Electronics Technology Co.). The sample was fabricated on an aluminum tube with Au electrodes and platinum wires. A Ni–Cr alloy wire through the tube was used as a heating filament. The volume of the testing chamber was 30 L, and two fans were used to make the test gas atmosphere homogeneous. The gas sensing tests were carried out at a humidity of 3%, and the operation temperatures were 150 and 190 °C. The response (S) was defined as the ratio of the sensor resistance in air (R_a) to that in testing gas (R_g), $S=R_a/R_g$.

Results and discussion

Figure 1 shows the TG curve of the $(PANI)_xMoO_3$ hybrid powder. Small weight loss for up to 300 °C is due to the

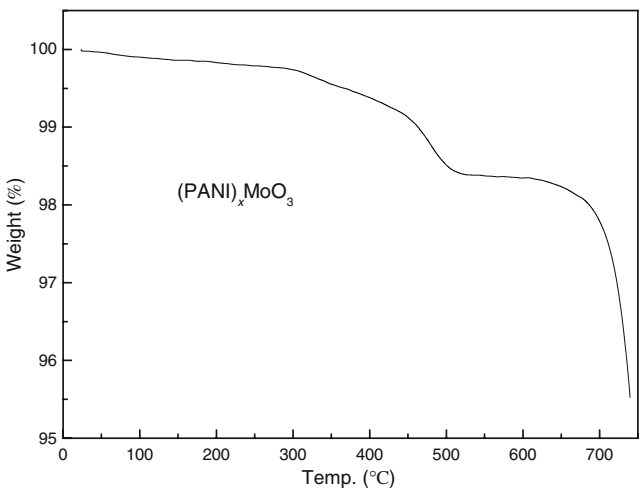

Fig. 1 TG patterns of the $(PANI)_xMoO_3$ hybrid in N_2

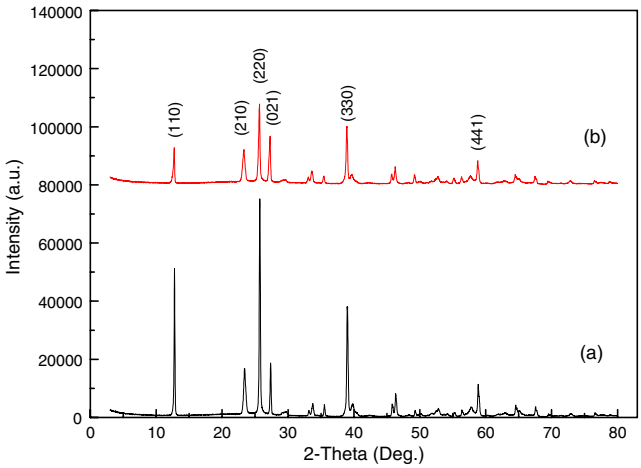

Fig. 2 X-ray diffraction pattern of MoO_3 xeogel (*a*) and $(PANI)_xMoO_3$ (*b*)

release of adsorbing water on the surface and interlayers. The thermal decomposition of the intercalated PANI attributes to large weight loss of 1.5% over 300 °C. Therefore, the temperature of heating hybrid power is less than 300 °C. In this work, the temperature of hybrid powder vacuum-dried was selected 50 °C, and the operation temperature of gas sensing tests was selected 150 and 190 °C.

Figure 2 shows the typical XRD patterns of MoO_3 xerogel and $(PANI)_xMoO_3$. It can be observed that the position of the characteristic peaks of the two products is consistent, whereas the peak intensity is different. The peak intensity of MoO_3 is much stronger than that of $(PANI)_xMoO_3$, indicating that the peak intensity decreases (Fig. 2 b) due to intercalation of polyaniline into layers of MoO_3. It shows that all the diffraction peaks can be indexed to the pure phase of MoO_3 with the orthorhombic structure (JCPDS: 65-2421), indicating that the products are of high purity.

Figure 3 shows the SEM images of the MoO_3 xerogel and $(PANI)_xMoO_3$ at different magnifications, respectively. Figure 3a is overall view of the MoO_3 xerogel at a relatively low magnification. It can be observed that a large number of long and uniform microrods are distributed homogeneously. The average length of the microrods is about 8–15 μm. A higher magnification image (Fig. 3b) shows that the diameter is approximately 0.5–1.0 μm. Figure 3c and d exhibits almost the same morphology with Fig. 3a and b, indicating that morphology of MoO_3 is not changed with polyaniline intercalated MoO_3 layers.

Figure 4 illustrates the charge–discharge curves of MoO_3 and $(PANI)_xMoO_3$ at a charge–discharge current density of 100 mA g^{-1}. The charge and discharge curves of two materials are similar. The discharge curves of pristine material show the voltage plateaus at 2.1–2.4 V, while the discharge curves of hybrid material show the voltage plateaus at 2.2–2.5 V, slightly higher than pristine material. Compared with pristine material, the length of the plateaus for hybrid material was increased, which resulted in higher specific discharge capacity. It can be observed

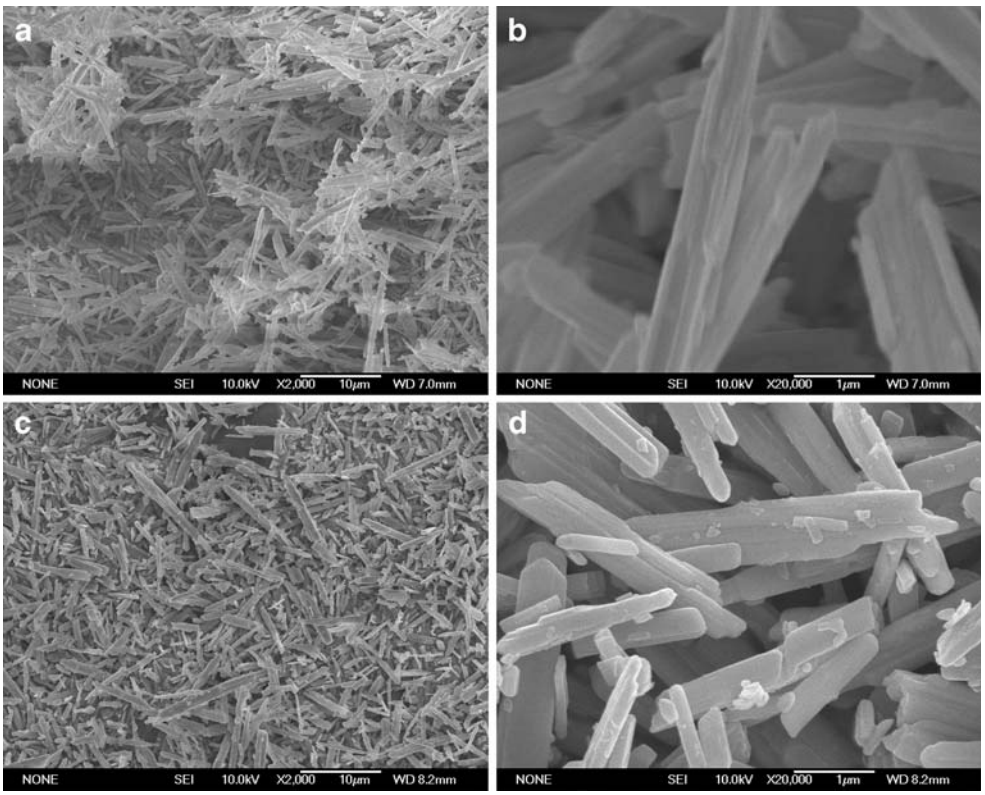

Fig. 3 Typical SEM images of the as-prepared MoO_3 (**a**, **b**) and $(PANI)_xMoO_3$ (**c**, **d**) at different magnifications

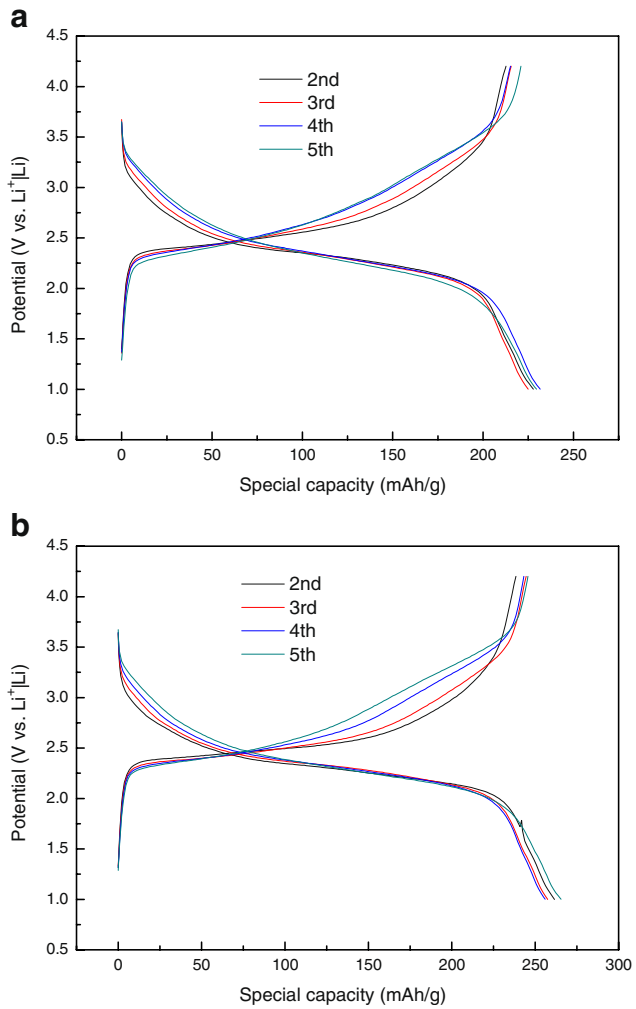

Fig. 4 Charge–discharge curves of MoO_3 (**a**) and $(PANI)_xMoO_3$ (**b**)

that the voltage difference of charge–discharge plateau for $(PANI)_xMoO_3$ (b) is smaller than that of MoO_3 (a) in corresponding cycle, indicating the better reversibility of cathode material after intercalated polyaniline.

Figure 5 shows that the curves of discharge capacity versus the cycle number for the electrode materials made from MoO_3 and $(PANI)_xMoO_3$. It can be observed that discharge capacity of $(PANI)_xMoO_3$ is much higher than that of MoO_3 xerogel. The first specific discharge capacity of hybrid material is 285.8 mA h g^{-1}, and after 20 cycles, it remains 205.4 mA h g^{-1}, while the first specific discharge capacity of MoO_3 xerogel is 256.6 mA h g^{-1}, and after 20 cycles, it become 186.6 mA h g^{-1}. It is indicated that polyaniline has improved the capacity and cycling stability of cathode materials.

The second cyclic voltammograms curves of the electrodes made from MoO_3 and $(PANI)_xMoO_3$ samples are shown in Fig. 6. In the cathodic polarization process of the second cycle for the electrodes made from MoO_3 and $(PANI)_xMoO_3$, one obvious peak was located at 2.56 and

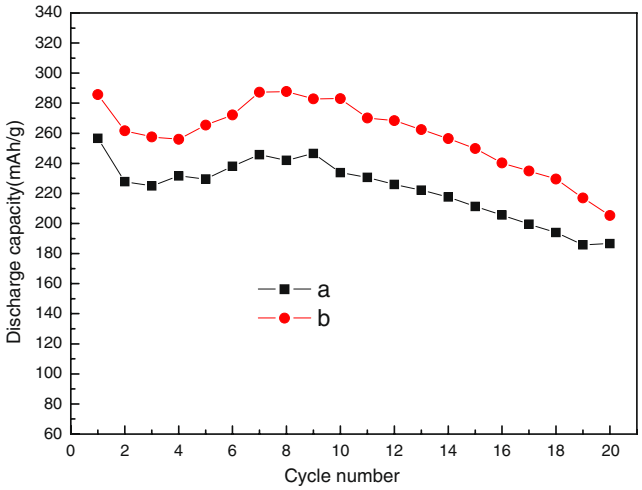

Fig. 5 Comparison of cycling stability curves of MoO_3 (*a*) and $(PANI)_xMoO_3$ (*b*)

2.64 V versus $Li^+|Li$, respectively, corresponding to the lithium intercalation processes; in the following anodic polarization, one strong peak was observed at 2.21 V and 2.26 V, respectively, corresponding to the lithium extraction processes. The area of CV curves for $(PANI)_xMoO_3$ is much larger than that for MoO_3, indicating much higher capacity of $(PANI)_xMoO_3$. It is consistent with the results of charge and discharge test shown in Fig. 5.

Figure 7 shows the ac impedance of cells with MoO_3 (a) and $(PANI)_xMoO_3$ (b) cathodes. The impedance spectrums show a high frequency semicircle and a low frequency tail, indicating the double layer response at the electrode/sample interface and the diffusion of lithium ions in the solid matrix. The impedance plots are fitted using the equivalent circuit model (Fig. 7c). The equivalent circuit model includes electrolyte resistance R_s, a constant phase element associated with the interfacial resistance, charge-transfer resistance R_{ct}, and the Warburg impedance (Z_w) related to

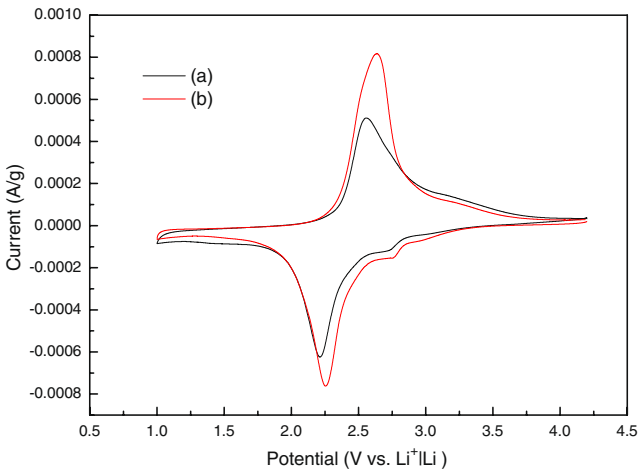

Fig. 6 Comparison of CV for the electrodes made from MoO_3 xerogel (*a*) and $(PANI)_xMoO_3$ (*b*) in the second cycle

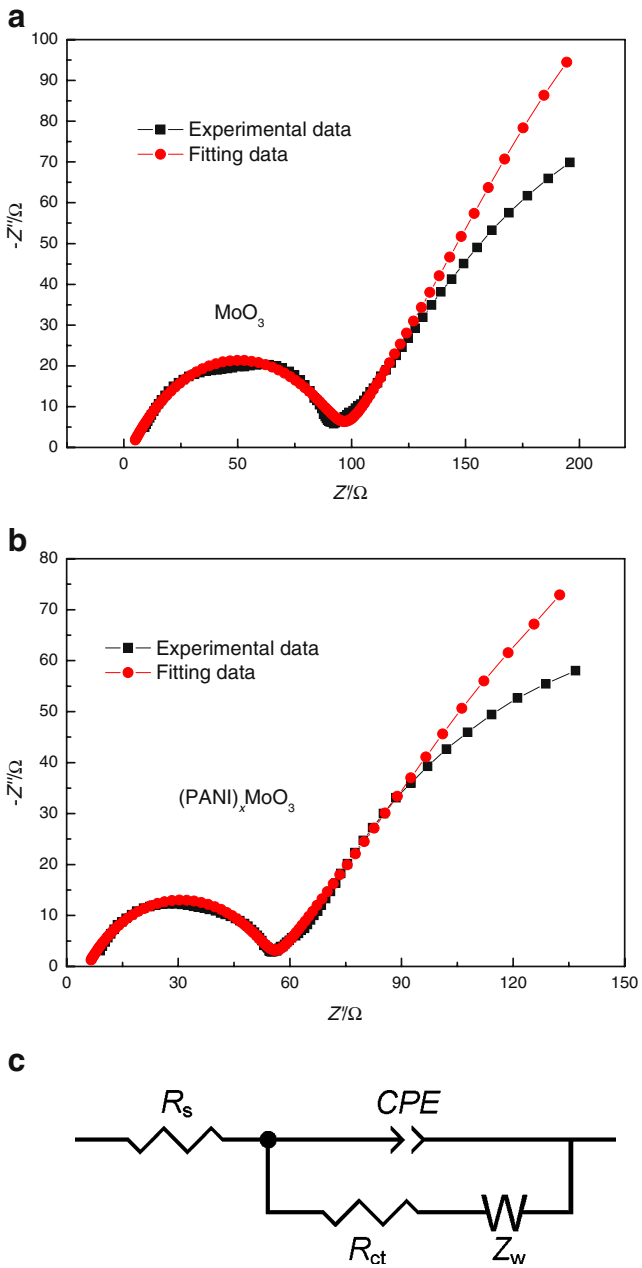

Fig. 7 Nyquist plots of MoO_3 xeogel (**a**) and $(PANI)_xMoO_3$ (**b**); equivalent circuit model (**c**)

the diffusion of lithium ions in the solid oxide matrix. According to Chen et al. studies on EIS of lithium-ion cells, cathode impedance is mainly attributed to the cell impedance, especially charge-transfer resistance [22]. Table 1 shows that the R_{ct} of $(PANI)_xMoO_3$ cathodes (50.10 Ω) is much smaller than the R_{ct} of MoO_3 (93.71 Ω). It indicates that oxidation–reduction reaction processes more easily and electronic conductivity increases. From Table 1, it also can be observed that the Z_w of $(PANI)_xMoO_3$ cathodes (313.2 Ω) is much smaller than the Z_w of MoO_3 (455.6 Ω). It indicates that the diffusion

Table 1 Comparison of EIS data for MoO_3 and $(PANI)_xMoO_3$

Sample	R_{ct} (Ω)	Z_w (Ω)
MoO_3	93.71	455.6
$(PANI)_xMoO_3$	50.10	313.2

of lithium ions processes more easily and diffusion velocity increases. It concludes that electrochemical performance of cathode material is improved after polyaniline intercalated into MoO_3 layers.

Figure 8 shows the comparative sensitivities of MoO_3 and $(PANI)_xMoO_3$ toward different concentration of ethanol at 150 and 190 °C, respectively. It can be observed that both two products are very sensitive to ethanol, and sensitivities are both improved with temperature increased. It shows that $(PANI)_xMoO_3$ hybrid material has better sensitive

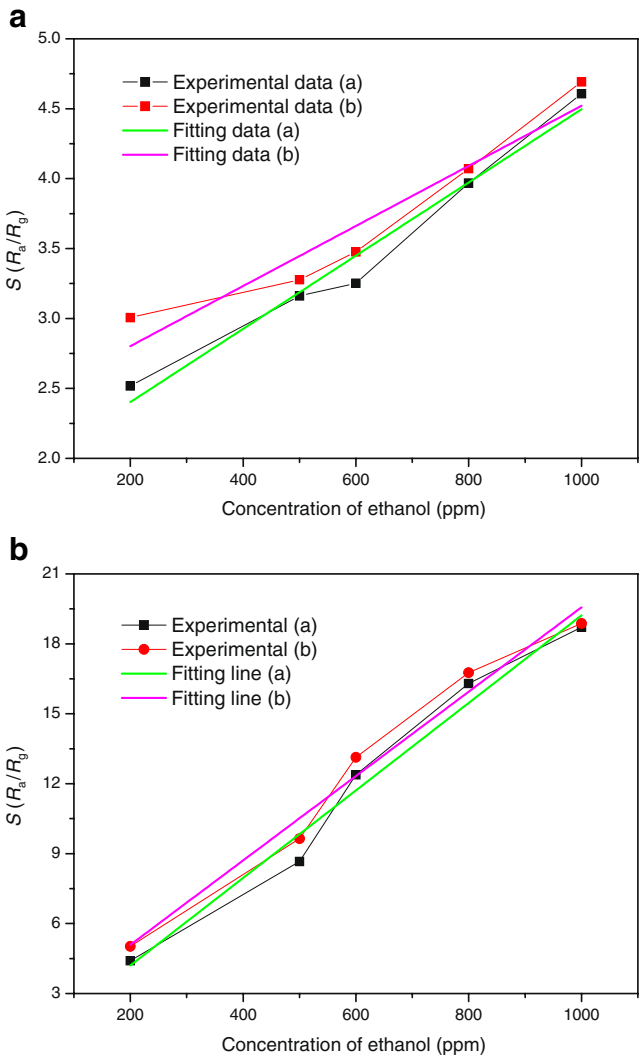

Fig. 8 Sensitivities of MoO_3 (*a*) and $(PANI)_xMoO_3$ (*b*) toward different concentration of ethanol at 150 °C (**a**) and 190 °C (**b**), respectively

performance to ethanol gas than MoO_3, indicating that interlayer spaces play an important part in the sensitiveness of cathode materials. Hybrid materials have large potential improvement in gas sensing and could probably be novel and promising gas sensitive materials.

Conclusions

In this paper, hybrid material of polyaniline with molybdenum trioxide (MoO_3) xerogel obtained by ion exchange of $(NH_4)_6Mo_7O_{24}{\cdot}4H_2O$ was successfully synthesized via polymerization of the monomer by ammonium peroxydisulfate/HCl oxidant system. Electrochemical measurements of lithium-ion batteries exhibited that $(PANI)_xMoO_3$ hybrid material showed a higher discharge capacity of 285.8 mA h g^{-1} and much lower charge-transfer resistance (50.10 Ω) than MoO_3 xerogel. Results showed that intercalation of polyanine improved the electrochemical performance of the cathode material. In addition, $(PANI)_xMoO_3$ hybrid material has better sensitivity to ethanol gas. Therefore, this kind of hybrid material is valuable to further research and could be a promising cathode material in lithium-ion batteries and potential gas sensing material.

Acknowledgments This work was supported by the Natural Science Fund of Tianjin (06YFJMJC04900), National Science Foundation of China (20673062, 20801059), and 973 program (2002CB 211800).

References

1. Kickelbick G (2003) Prog Polym Sci 28:83. doi:10.1016/S0079-6700(02) 00019-9
2. Gagopadhyay R, De A (2000) Chem Mater 12:608. doi:10.1021/cm990537f
3. Yu O, Posudievsky SA, Biskulova DA, Pokhodenko VD (2002) J Mater Chem 12:1446. doi:10.1039/b111187f
4. Gomez-Romero P (2001) Adv Mater 13:163. doi:10.1002/1521-4095(200102) 13:3<163::AID-ADMA163>3.0.CO;2-U
5. Fusalba F, Bélanger D (2000) Electrochim Acta 45:3877. doi:10.1016/S0013-4686(00) 00454-0
6. Kuwabata S, Idzu T, Martin CR, Yoneyama H (1998) J Electrochem Soc 145:2707. doi:10.1149/1.1838702
7. Shen PK, Huang HT, Tseung ACC (1992) J Electrochem Soc 139:1840. doi:10.1149/1.2069508
8. Asim N, Radiman S, Yarmo MA (2008) Mater Lett 62:1044. doi:10.1016/j.matlet.2007.07.051
9. Stilwell DE, Park SM (1988) J Electrochem Soc 135:2491. doi:10.1149/1.2095364
10. Rahman MA, Kumar P, Park D, Shim Y (2008) Sensors 8:118. doi:10.3390/s8010118
11. Spahr ME, Novak P, Haas O, Nesper R (1995) J Power Sources 54:346. doi:10.1016/0378-7753(94) 02099-O
12. Dobay R, Harsanyi G, Visy C (1999) Electroanalysis 11:804. doi:10.1002/(SICI) 1521-4109(199907) 11:10/11<804::AID-ELAN804>3.0.CO;2-B
13. Giulio MD, Manno D, Micocci G, Serra A, Tepore A (1998) Phys Status Solidi 168:249. doi:10.1002/(SICI) 1521-396X(199807) 168:1<249::AID-PSSA249>3.0.CO;2-9
14. Ferroni M, Guidi V, Martinelli G, Sacerdoti M, Nelli P, Sberveglieri G (1998) Sens Actuator B 48:285. doi:10.1016/S0925-4005(98) 00057-4
15. Imawan C, Steffes H, Solzbacher F, Obermeier E (2001) Sens Actuator B 77:346. doi:10.1016/S0925-4005(01) 00732-8
16. Stejskal J, Gilbert RG (2002) Pure Appl Chem 74:39. doi:10.1351/pac200274050857
17. Ballav N, Biswas M (2006) Mater Lett 60:514
18. Itoh T, Matsubara I, Shin W (2008) Mater Chem Phys 110:115. doi:10.1016/j.matchemphys.2008.01.024
19. Liu XX, Bian LJ, Zhang L, Zhang LJ (2007) J Solid State Electrochem 11:1279. doi:10.1007/s10008-007-0287-3
20. Wang JZ, Matsubara I, Murayama N, Woosuck S, Izu N (2006) Thin Solid Films 514:329. doi:10.1016/j.tsf.2006.02.030
21. Huang JX, Virji S, Wheiller BH, Kaner RB (2003) J Am Chem Soc 125:314. doi:10.1021/ja028371y
22. Chen CH, Liu J, Amine K (2001) J Power Sources 96:321. doi:10.1016/S0378-7753(00) 00666-2